

Analysis of the Seismic Behaviour of Propped Retaining Structures

Luigi Callisto¹, Fabio M. Soccodato² and Riccardo Conti³

¹University of Rome 'La Sapienza', Italy; luigi.callisto@uniroma1.it

²University of Cagliari, Italy; soccodato@unica.it

³University of Rome 'Tor Vergata', Italy

ABSTRACT: This paper discusses the results of a dynamic numerical analysis in which a pair of propped retaining walls embedded in a dry coarse-grained soil are subjected to two different earthquakes. The retaining walls have a small embedded length, so that they undergo significant displacements under seismic conditions. Soil behaviour is described with a non-linear elastic-plastic model, with damping resulting from irreversible strains. The seismic input is made of two real acceleration time histories, having a similar Arias intensity but a different frequency content. The response of the soil and the retaining structures to these different inputs is presented, devoting a special attention to the description of soil-wall interaction that occurs during an earthquake.

INTRODUCTION

The mechanical behaviour of embedded retaining structures subjected to seismic loading is still unclear, as it results from a combination of phenomena which can be difficult to model with sufficient accuracy. During the propagation of seismic waves through a continuum in which an excavation has been made, a bi-dimensional amplification occurs, which depends on the spatial distribution of stiffness, on the non-linear soil response and on the hysteretic soil behaviour. Because of the excavation, a significant portion of the soil located in the vicinity of the retaining walls is in a state close to limit equilibrium, and this in turn affects the soil response to the subsequent seismic loading. It follows that a pre-requisite for a reasonable prediction of the seismic behaviour of these structures is a reliable estimate of the stress state produced by the excavation. This poses certain constraints to the constitutive models that can be deemed adequate to study this problem: beyond being able to reproduce non-linearity and hysteretic damping, they should allow for the development of plastic limit conditions.

The seismic design of embedded retaining structures is routinely performed using a pseudo-static approach, in which a constant acceleration field is superimposed to

the gravity acceleration, and safety against a collapse mechanism is checked using limit equilibrium methods. When it comes to the use of more advanced analyses, which account for the variation of acceleration in space and time, the notion of safety against a collapse mechanism becomes meaningless and attention should especially be focused on the permanent displacements undergone by the geotechnical system.

A preceding paper (Callisto & Soccodato 2007) presented the results obtained from an analysis of an ideal pair of cantilever embedded retaining walls subjected to a real acceleration time history. The present paper is aimed to extend this investigation to the case of embedded retaining walls connected to each other by a prop level, subjected to two different seismic inputs.

NUMERICAL MODEL AND SEISMIC INPUT

The dynamic analysis was carried out using the Finite Difference Code FLAC v.5 (Itasca 2005). Figure 1 shows the finite difference grid, together with a schematic layout of the retaining structures. An ideal excavation with a depth of 4 m is supported by a couple of embedded retaining walls connected to each other by an elastic prop hinged at the top. The excavation is carried out in a dry coarse-grained soil with a constant angle of friction $\phi' = 35^\circ$, density $\rho = 2.04 \text{ Mg/m}^3$ and a stress-dependent small strain shear modulus $G_0 = 10000 \cdot p'^{0.5}$ (kPa), where p' is the mean effective stress. The bedrock is located at a depth of 30 m from the ground surface. Table 1 lists the values of the key input parameters for the analysis.

The embedded length of the walls, equal to 1.5 m, was computed through a pseudo-static limit equilibrium analysis in which a horizontal seismic coefficient $k_h = 0.1$ was used and a global factor of safety equal to 1.8 was applied to the passive resistance. Active seismic forces were evaluated using the Mononobe-Okabe (M.O.) theory, while the passive ones were computed, assuming a soil-wall angle of friction $\delta = 20^\circ$, with the solution developed by Lancellotta (2007) based on a lower bound limit analysis.

Soil behaviour was described using a non-linear model with hysteretic damping available in the FLAC library. This model is a two-dimensional extension of the one-dimensional non linear models describing hysteresis loops through the Masing (1926) rules; details are given in Itasca (2005). The model parameters were chosen to reproduce the Seed & Idriss (1970) modulus decay and damping curves for sands, as discussed by Callisto & Soccodato (2007). This hysteretic model was used to update at each calculation increment the shear modulus of an elastic-perfectly plastic soil model with a Mohr-Coulomb failure criterion and a non-associated flow rule (dilatancy angle $\psi = 0$). Therefore, plastic strains associated to full strength mobilisation occurring during the analysis provided additional energy dissipation beyond that resulting from the Masing rule. No additional viscous damping was introduced in the analysis.

The soil-wall contact was simulated using elastic-perfectly plastic interfaces with a friction angle $\delta = 20^\circ$. A small cohesion $c' = 0.5 \text{ kPa}$ was used to ensure numerical stability in the calculation.

Zones in the finite difference grid have a size of 0.25 m near the retaining wall

and a maximum size of 1.2 m in the vicinity of the bedrock. The initial stress state was computed assuming an earth pressure coefficient at rest $K_0 = 0.5$. Effects of the installation of the retaining walls were not modelled. The static analysis for the excavation was carried out in four steps, each time removing 1 m of soil; the prop was installed at the beginning of the excavation. In this calculation a reduced shear modulus was used, equal to $0.3 G_0$, corresponding on the Seed & Idriss (1970) modulus decay curve to a shear strain $\gamma \approx 0.1 \%$. During the static stage, the grid was restrained horizontally and vertically at the base, while only horizontal displacements were prevented on the lateral sides.

The dynamic analysis was carried out applying acceleration time-histories to the bedrock nodes. On the lateral sides, standard FLAC dynamic boundary conditions were applied: the grid was connected to “quiet” boundaries (Lysmer & Kuhlemeyer, 1969) that in turn were connected to free-field boundaries, along which a free-field one-dimensional calculation was carried out in parallel with the main grid calculation. The time increment used in the explicit time integration scheme was $\Delta t = 2 \cdot 10^{-7}$ s.

Two real seismic signals recorded in Italy on stiff soils were applied to the bottom boundary of the grid, namely the Tolmezzo (TM) and the Assisi (AS) acceleration time histories. The Tolmezzo record has a peak acceleration $a_{\max} = 0.35$ g and an Arias intensity $I_a = 0.79$ m/s. The Assisi record was scaled to $a_{\max} = 0.28$ g to obtain a similar Arias intensity as the Tolmezzo record. The significant durations (between 5 and 95 % of I_a) are of 9.9 and 10.5 s respectively. The input signals were low-pass filtered at 15 Hz for compatibility with the dimensions of the larger grid zones. Their Fourier amplitude spectra signals are shown in Figure 2(a,f) where it is apparent that the two records are characterised by a different frequency content: the Tolmezzo time history shows significant Fourier amplitudes in the range of 1 to 4 Hz, while the Assisi time history shows the highest amplitudes between 2.5 and 6 Hz. The mean period T_m as defined by Rathje et al. (1998) is equal to 0.4 and 0.24 s respectively.

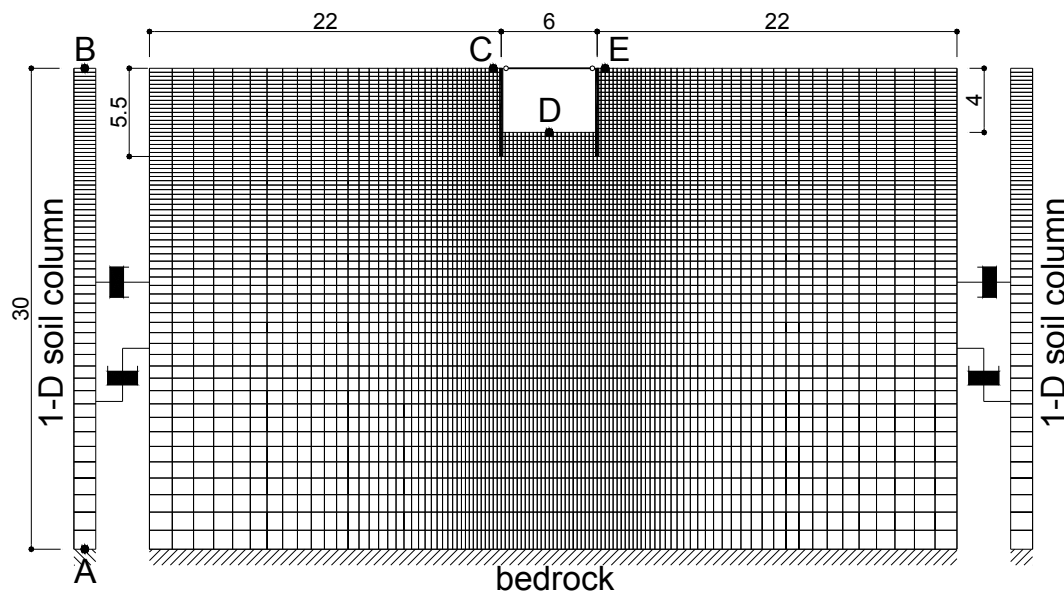


FIG. 1. Problem layout and finite difference grid.

Table 1. Input parameters for the analysis.

ρ (Mg/m ³)	c' (kPa)	ϕ' (°)	ψ	δ (°)	G_0 (kPa)	ν'	retaining walls		prop level
							EA (kN/m)	EI (kNm ² /m)	EA (kN/m)
2.04	0.5	35	0	20	10000· $p'^{0.5}$	0.2	1.21·10 ⁷	2.72·10 ⁵	3.0·10 ⁶

RESULTS

Amplification

Table 2 reports some properties of the acceleration time histories computed at specific locations, while the corresponding Fourier spectra are shown in Figure 2. A significant amplification is obtained for $f = 2$ Hz, which is about the fundamental frequency of the deposit. Frequencies in the range of 4 to 6 Hz are also amplified, especially in the soil zones located behind the retaining wall, near the stiff support system. The overall frequency content is modified only slightly by amplification, as shown by the values of the mean period T_m .

For both input records, one-dimensional propagation produces a three-fold increase in the Arias intensity (from 0.79 to 2.4-2.5 m/s). Additional amplification is produced by two-dimensional effects, as shown by a further increase in the Arias intensity close to the retaining walls; this effect is substantial for the Assisi input record, which yields Arias intensities as high as 6.2 m/s. In general, properties of the acceleration time histories computed at points C and E, behind the two retaining walls, are very similar to each other.

The Fourier spectra of Figure 2 show that the computed acceleration time histories contain non-zero amplitudes at large frequencies that are not present in the input records. This effect may be ascribed to insufficient damping produced by the hysteretic soil model at small strains, and might be corrected by introducing a small viscous damping in the analysis. However, a spectral analysis of the displacement time histories of the walls and of the adjacent soil showed that such high frequencies do not produce any additional permanent displacement, therefore their effect appears negligible for practical purposes.

Stress state

Figure 3 shows the distribution of the total horizontal stress σ_h acting against the retaining walls. The figure also shows the theoretical distributions of σ_h for active and passive limit states, evaluated using the static active and passive earth coefficients K_a and K_p obtained by Lancellotta (2002) (solid lines). Under static conditions, active limit state is attained behind the retaining walls down to about 3.5 m, while larger values of σ_h are computed below this depth. In front of the walls, full mobilization of passive resistance is observed down to about 4.5 m, i.e. 0.5 m below the bottom, essentially due to the decrease in vertical stress produced by the excavation. A more complete illustration of the stress state under static conditions can be seen in the plot of Figure 4(a) which shows, for the central part of the grid,

Table 2. Properties of acceleration time histories computed at specific locations.

input signal	Tolmezzo					Assisi				
location	A	B	C	D	E	A	B	C	D	E
a_{\max} (g)	0.35	0.56	0.93	0.72	0.67	0.28	0.51	1.15	1.25	1.05
I_a [12s] (m/s)	0.79	2.36	3.73	2.24	3.71	0.79	2.54	6.17	2.32	6.24
T_m (s)	0.40	0.46	0.39	0.44	0.39	0.24	0.26	0.23	0.24	0.23
$f_m = T_m^{-1}$ (Hz)	2.50	2.17	2.56	2.27	2.56	4.17	3.84	4.35	4.17	4.35

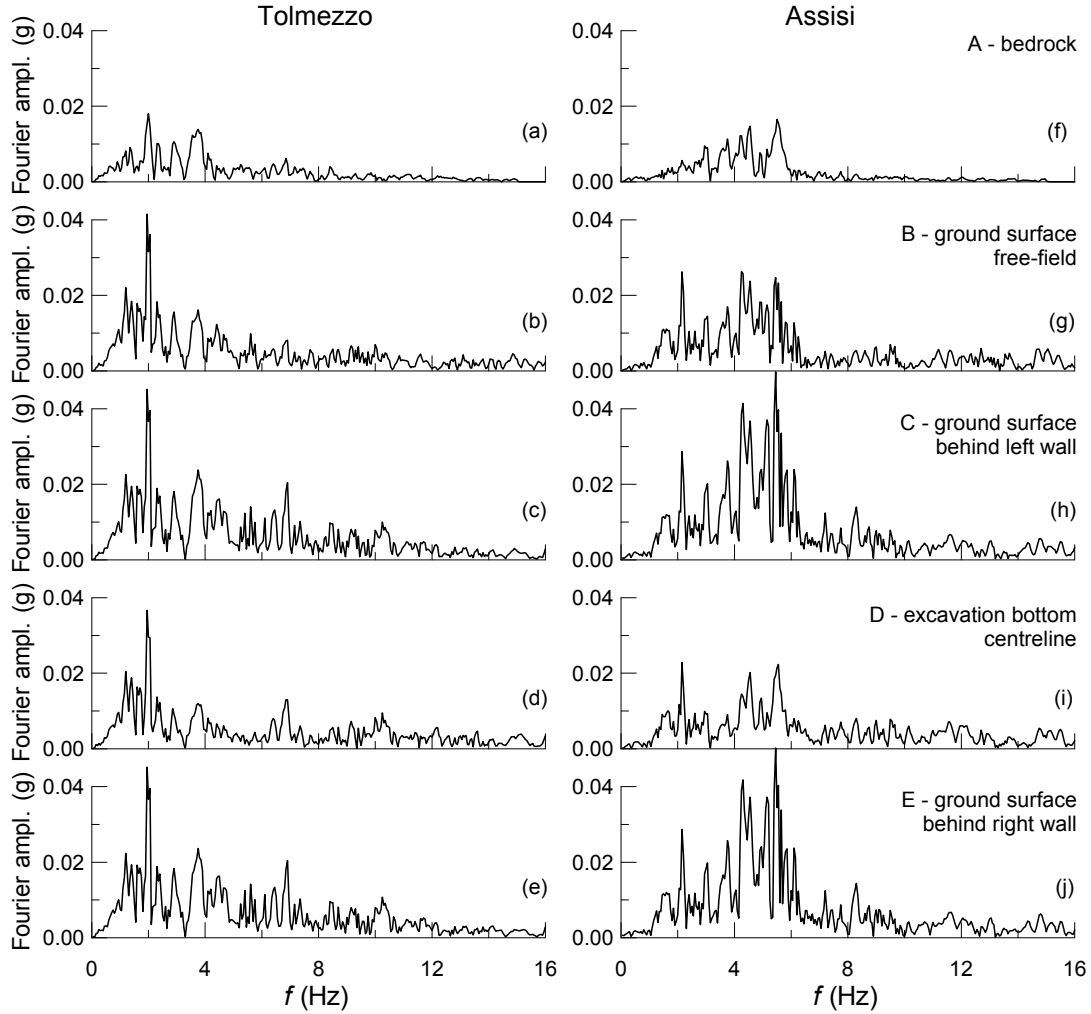


FIG. 2. Fourier spectra of the acceleration time histories computed at specific locations (see Fig. 1).

the contours of the mobilised strength, defined as the ratio τ/τ_{lim} of the maximum shear stress acting at a point and the corresponding available strength.

During the earthquake, the normal stresses acting against the wall change very rapidly in a somewhat erratic way. Nevertheless it is possible to observe specific trends in the distribution of the contact stresses, and these are shown in Figure 3(a) at the selected instants of 5.0 s and 5.8 s for the analyses involving the Tolmezzo and the Assisi record respectively. At these instants, contact stresses against the left wall

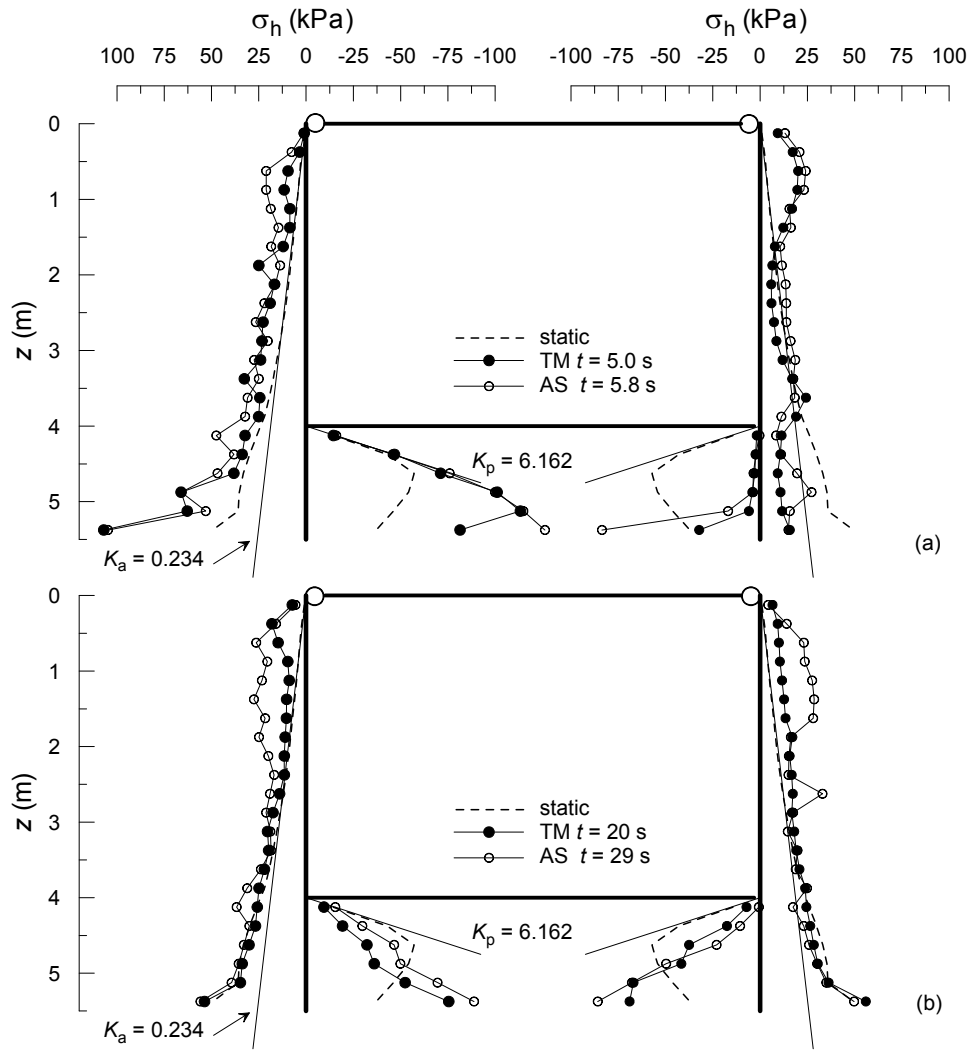


FIG. 3. Computed horizontal stresses acting against the retaining walls during (a) and after (b) the earthquakes.

are the highest. This implies a low mobilisation of shear strength behind the wall, and an almost full mobilisation of shear strength in front of the wall. Conversely, at the same instants, contact stresses acting against the right wall are the lowest, and this in turn implies full mobilisation of shear strength behind the wall and a 90 degrees rotation of the principal stress directions in front of the wall, where near active limit conditions are attained. During strong motion, contact stresses increase and decrease simultaneously behind and in front of a single wall, and this behaviour occurs in an alternate fashion between the two walls. It is interesting to note that during shaking the contact stresses behind the upper part of the walls become much higher than those computed under static conditions. This effect, which was not observed in the seismic analysis of cantilever walls (Callisto & Soccodato 2007) is probably caused by the stiff prop restraining the relative displacements at the top of the walls. Figure 4(b) shows the contour plot of τ/τ_{lim} for the Tolmezzo earthquake at $t = 5$ s. It can be seen that behind the walls there is a spreading of the plastic zones

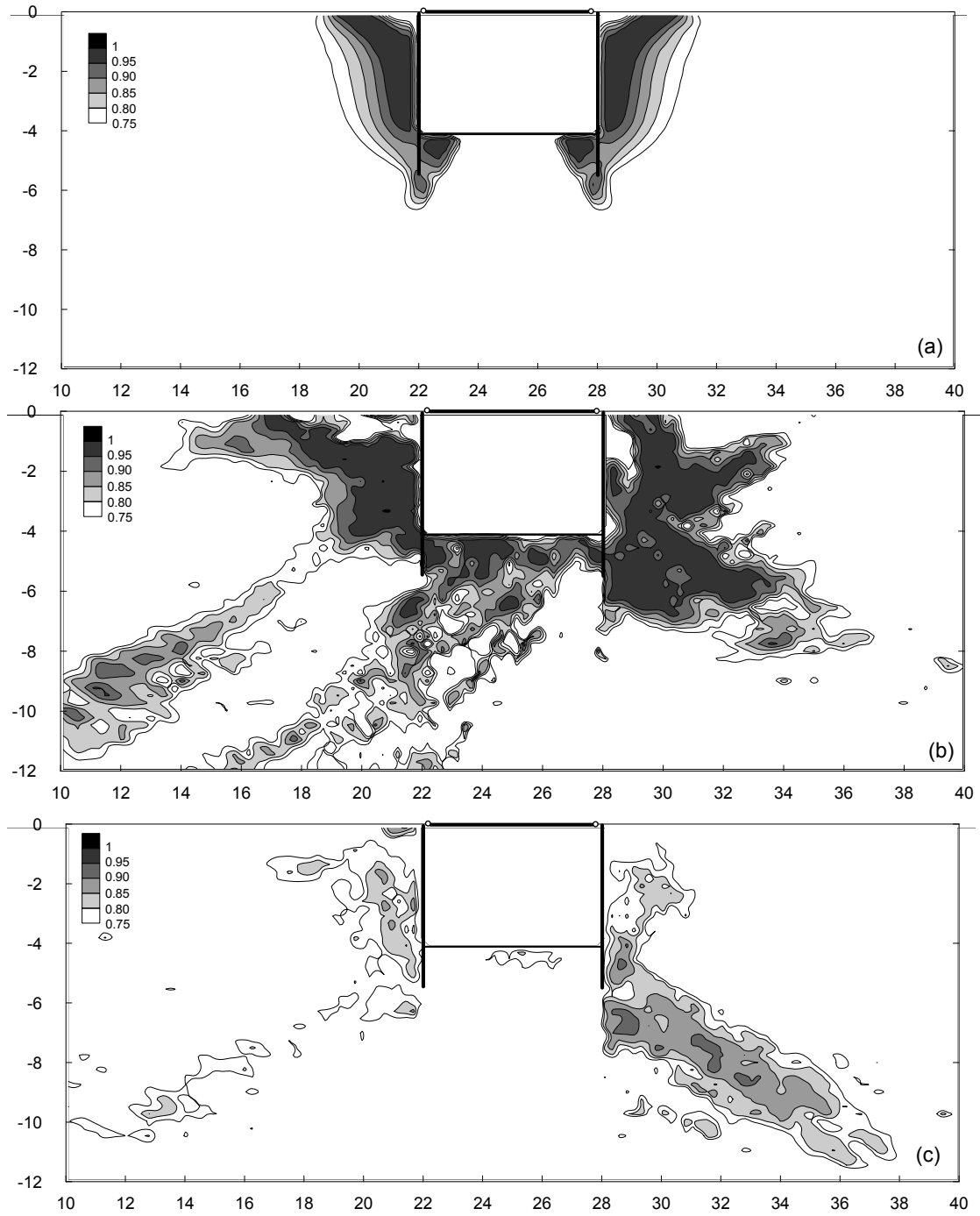


FIG. 4. Contours of the mobilised shear strength in static conditions (a); after 5 s of the Tolmezzo record (b); at the end of the Tolmezzo record (c).

($\tau/\tau_{\text{lim}} > 0.95$) that assume wedge-like shapes, while the soil in front of the left wall is close to passive limit conditions, consistent with the distribution of σ_h depicted in Fig. 3(a). Note that the plastic zones extend well below the toe of the right wall: the toe is moving towards the excavation (see next section) and this causes a perturbation which is spread downwards because of soil continuity. This is quite different from

the results obtained for a pair of cantilevered walls, in that for such walls the toe was close to the instantaneous rotation point undergoing very small displacements, and the plastic zones were thus confined to an upper portion of soil.

At the end of the earthquake, symmetry in the distribution of σ_h is nearly restored for the Assisi earthquake (Figure 3(b)). Conversely, at the end of the Tolmezzo record σ_h values behind the left wall near the prop are significantly larger than those acting against the right wall. Contact stresses in front of the walls show a quasi-linear distribution and are about half of the available static passive pressures: if compared to the initial static conditions, the soil in the lower part of the wall is closer to a limit passive state, while soil elements located right below the bottom of the excavation are more distant from passive conditions. The contour plot of Figure 4(c) shows that the soil stress state is now everywhere quite far from a plastic limit state and therefore, in terms of a limit equilibrium analysis, a collapse mechanism appears to be more distant than in the initial conditions. However, this also implies that the net pressures acting against the walls are larger and therefore stresses in the walls are more significant, as discussed in the next section.

Bending moments and axial force

Figure 5 shows the spatial and temporal variation of the bending moments M in the walls and the axial force N in the prop. In static conditions, the computed values of M and N are in a close agreement with those obtained from the limit equilibrium calculation. Seismic shaking produces a significant increment in both M and N , which is seen to occur in a rather different way for the two seismic records: the Tolmezzo earthquake results in a few sharp peaks in M and N occurring between 4 and 6 s, after which both M and N stabilize to somewhat lower values; conversely, the increase in M and N produced by the Assisi earthquake is more gradual, and the final values are quite higher. The post-seismic distribution of bending moments after the Tolmezzo earthquake could be obtained with a pseudostatic analysis using a seismic coefficient $k_h = 0.16$, and this was shown to be the case also for a pair of cantilevered walls. However, the resulting value of the axial force in the prop would be about 30 % smaller than that computed in the numerical analysis. The Assisi earthquake, with a similar Arias intensity and a lower peak acceleration, is seen to be much more damaging for this specific problem.

Displacements

Figure 6 shows the horizontal displacements u of the retaining walls, relative to the free-field lateral boundaries, and the settlements w of the soil located behind the walls, computed at the end of the earthquake. The seismic events produce permanent horizontal displacements of the walls which are an order of magnitude larger than the very small static ones. After the Assisi earthquake symmetrical wall displacements are computed, consisting in a quasi-rigid rotation about the propped top. The ground surface settles accordingly, with maximum vertical displacements occurring right behind the walls. A different behaviour is observed after the Tolmezzo record, whose

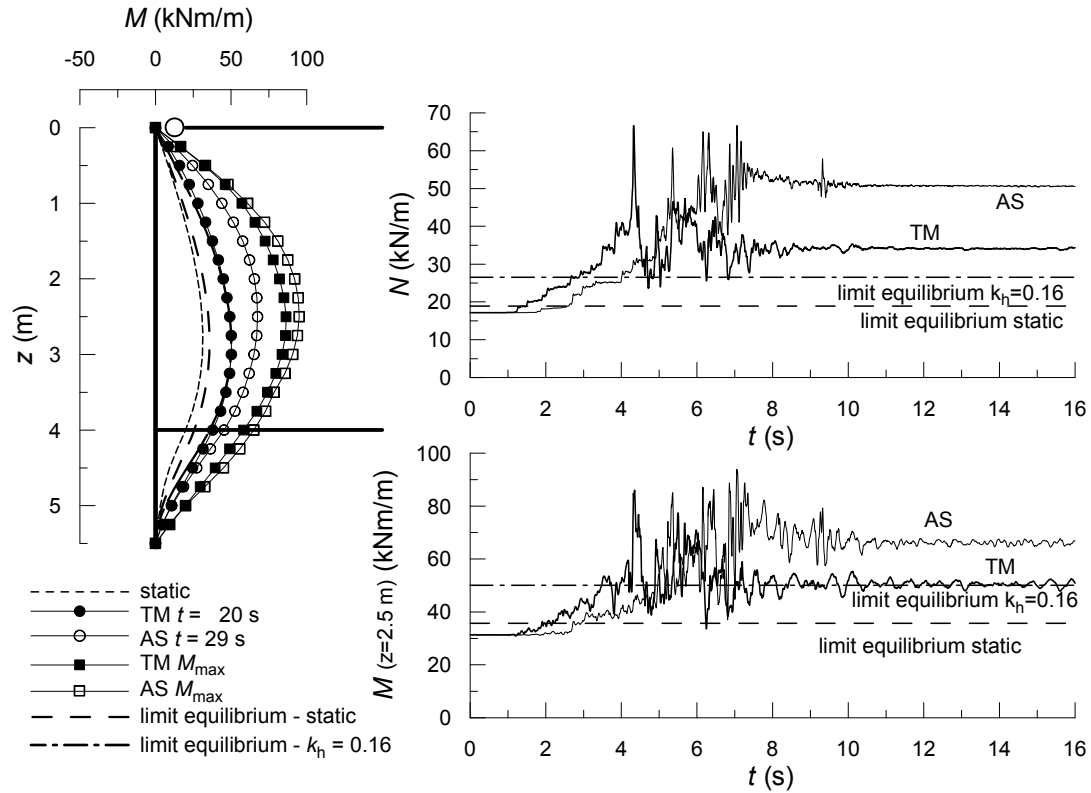


FIG. 5. Spatial and temporal variation of bending moments M in the wall and axial force N in the prop.

displacement time history is strongly unsymmetrical: after this earthquake the right wall has translated towards the excavation while the left wall shows a rotation about its toe, with permanent displacements directed away from the excavation. Consistently, settlements behind the right wall are larger than those occurring close to the left wall, and are spread to a larger distance from the excavation.

CONCLUSIONS

Propagation of the two seismic records in the vicinity of a pair of propped retaining walls causes instantaneous attainments of the available shear strength in soil zones interacting with the walls, resulting in a progressive increase in bending moments and axial force, and in a gradual accumulation of displacements.

The two real acceleration time histories, applied to the lower boundary of the finite difference grid, are both significantly amplified and this amplification appears to be emphasized by a two-dimensional interaction with the excavation. The Assisi record, characterized by a similar Arias intensity as the Tolmezzo record and by a smaller peak acceleration, causes the strongest effects, particularly in terms of stresses in the walls and in the prop. This may be related to its higher frequency content, and to the consequent larger amplification occurring close to the stiff structures supporting the excavation.

The bedrock seismic input chosen for these analyses is quite severe and would correspond to an ultimate limit state for the worst scenario in the Italian territory.

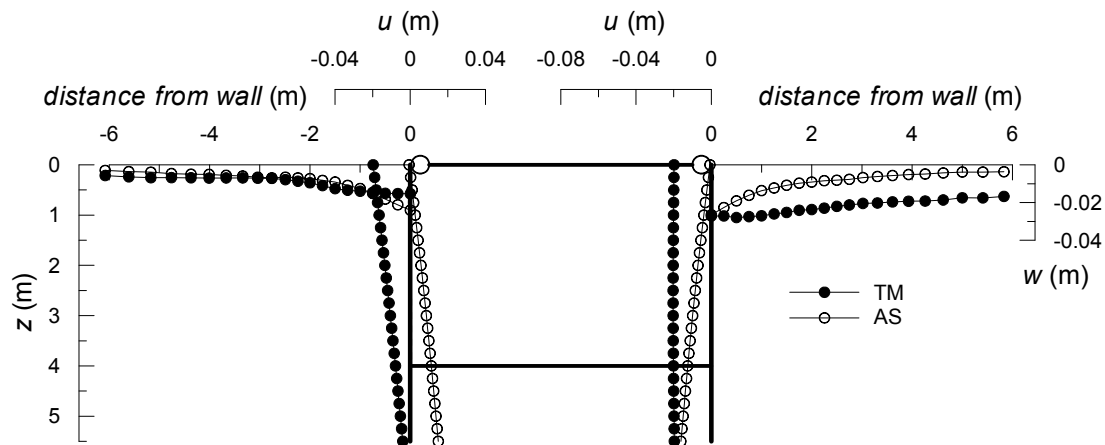


FIG. 6. Computed displacements of retaining walls and ground surface.

Nevertheless the retaining walls, proportioned using a pseudo-static approach with seismic coefficients equal to only a fraction (29-35 %) of the peak bedrock acceleration, undergo displacements smaller than 30 mm, while they are subjected to bending moments that during shaking might produce instantaneous yielding. The most critical component seems to be the prop, with respect to normal stresses and to safety against buckling, since at the end of the Assisi earthquake the prop level is subjected to a compressive axial force equal to about 2.5 times the initial one.

ACKNOWLEDGMENTS

The work presented in this paper is part of the *ReLUIS* research project, funded by the Italian Department of Civil Protection.

REFERENCES

- Callisto L. and Soccodato F.M. (2007). Seismic analysis of an embedded retaining structure in coarse-grained soils. *Proc. 4th Int. Conf. on Earthquake Geotechnical Engineering*. Thessaloniki.
- Itasca (2005). *FLAC Fast Lagrangian Analysis of Continua v. 5.0*. User's Manual.
- Lancellotta R. (2002). "Analytical solution of passive earth pressure". *Géotechnique*, 52 (8): 617-619.
- Lancellotta R. (2007). "Lower bound approach for seismic passive earth resistance". *Géotechnique*, 57 (3): 319-321.
- Lysmer, J., and Kuhlemeyer R.L. (1969). "Finite dynamic model for infinite media", *Journal of Engineering Mechanics* 95 (EM4): 859-877.
- Masing, G. (1926). "Eigenspannungen und Verfertigung beim Messing". *Proceedings 2nd Int. Congress on Applied Mechanics*, Zurich.
- Rathje E.M., Abrahamson N.A. and Bray J.D. (1998). Simplified frequency content estimates of earthquake ground motions. *Journal of geotech. and geoenv. eng.* 124 (2): 150-159.
- Seed H.B. and Idriss I.M.(1970). *Soil moduli and damping factors for dynamic analysis*. Report No. EERC 70-10, University of California, Berkeley, 1970.